Direct visualization of superselective colloid-surface binding mediated by multivalent interactions

Linne, Christine; Visco, Daniele; Angioletti-Uberti, Stefano; Laan, Liedewij; Kraft, Daniela J.

DOI
10.1073/pnas.2106036118

Publication date
2021

Document Version
Final published version

Published in
Proceedings of the National Academy of Sciences of the United States of America

Direct visualization of superselective colloid-surface binding mediated by multivalent interactions

Christine Linne[a,b], Daniele Visco[c,d], Stefano Angioletti-Uberti[c,d], Liedewij Laan[b,1], and Daniela J. Kraft[a,1]

[a]Soft Matter Physics, Huygens-Kamerlingh Onnes Laboratory, Leiden Institute of Physics, 2300 RA Leiden, The Netherlands; [b]Department of Bionanoscience, Technical University Delft, 2629 HZ Delft, The Netherlands; [c]Department of Materials, Imperial College London, SW72AZ London, United Kingdom; and [d]Thomas Young Centre, Imperial College London, SW72AZ London, United Kingdom

Edited by David A. Weitz, Harvard University, Cambridge, MA, and approved July 13, 2021 (received for review April 1, 2021)

Reliably distinguishing between cells based on minute differences in receptor density is crucial for cell–cell or virus–cell recognition, the initiation of signal transduction, and selective targeting in directed drug delivery. Such sharp differentiation between different surfaces based on their receptor density can only be achieved by multivalent interactions. Several theoretical and experimental works have contributed to our understanding of this "superselectivity." However, a versatile, controlled experimental model system that allows quantitative measurements on the ligand–receptor level is still missing. Here, we present a multivalent model system based on colloidal particles equipped with surface-mobile DNA linkers that can superselectively target a surface functionalized with the complementary mobile DNA-linkers. Using a combined approach of light microscopy and Foerster resonance energy transfer (FRET), we can directly observe the binding and recruitment of the ligand–receptor pairs in the contact area. We find a nonlinear transition in colloid-surface binding probability with increasing ligand or receptor concentration. In addition, we observe an increased sensitivity with weaker ligand–receptor interactions, and we confirm that the timescale of binding reversibility of individual linkers has a strong influence on superselectivity. These unprecedented insights on the ligand–receptor level provide dynamic information into the multivalent interaction between two fluidic membranes mediated by both mobile receptors and ligands and will enable future work on the role of spatial–temporal ligand–receptor dynamics on colloid-surface binding.

multivalent interactions | DNA-coated colloids | surface adhesion | superselectivity | binding kinetics

Processes at biological interfaces are often governed by multivalent interactions. They play a key role in signal transduction through inhibition and activation of signaling complexes and recognition and interactions between viruses and cells, as well as cell–cell adhesion (1–5). Multivalent bonds consist of a large number of weak bonds instead of a single strong one, which creates an interaction that is not only strong but also highly selective. The selectivity in multivalent systems goes beyond the correct recognition of a single ligand–receptor pair and allows "superselective" binding only to surfaces that exceed a critical receptor concentration. This allows for a sharp differentiation of surfaces that consist of the same receptor type but vary in receptor density. Integrating this powerful feature into drug delivery systems would enable highly selective targeting of diseased cells (6–8): for example, in cancer therapy (9–11) where tumor cells overexpress receptors on their surface (12, 13) or to target viral infections (14).

For multivalent recognition and particle uptake in biological settings, as well as for applications such as directed drug delivery, the binding affinity to the target surfaces needs to be precisely tuned. To this end, the bond should be selective and strong yet weak enough to be reversible to, for example, facilitate endocytosis (15). Specifically, theoretical studies have shown that the ligand density as well as interaction strength needs to be adjusted with respect to the receptor density to increase the selective surface binding (16–18). In addition, receptor mobility on the target surface—a key feature of membranes—leads to receptor clustering that can enhance the surface binding at low receptor concentrations (19–21).

These theoretical predictions have inspired the design of various experimental systems that can be used to investigate superselective surface binding. The ideal system for understanding superselectivity in biological context should mimic the lateral mobility of the ligands and receptors and provide full control over their interaction strength and surface densities, as well as yield quantitative insights into the bond formation and dynamics. Experimentally, superselective surface binding has been demonstrated for systems that consisted of ligand-bearing polymers (19, 22, 23), DNA-coated particles (20, 24), and influenza virus particles (25), as well as small unilamellar vesicles (SUVs) and giant unilamellar vesicles (21). These experiments confirmed theoretical predictions that a low binding affinity and high valency are crucial for obtaining superselectivity and furthermore, showed that lateral mobility of receptors on the target surface can induce clustering of the ligands or receptors in the bond area, which enhances superselectivity (19).

However, despite these intriguing observations, to date no system exists that captures the key features of biological interfaces, with both mobile ligands and receptors hosted by a lipid membrane, nor one that combines fluidic interfaces and the possibility for direct visualization of binding dynamics with a tunable interaction strength and ligand–receptor densities. This lack of a fully tunable model system prevents us from developing a

Significance

Multivalent interactions are an ensemble of multiple weak bonds that in a concerted effort can create a strong bond. Multivalent interactions often mediate adhesion in biological systems, where receptors and ligands are typically integrated in a fluidic membrane and thus laterally mobile on the surface. A characteristic property of multivalency is superselectivity: the ability to distinguish between surfaces based on receptor density. The results shown in this study provide quantitative insight into superselective binding of surface mobile receptors and ligands, important for adhesion to biological interfaces and applications, such as the design of drug delivery platforms.

Author contributions: C.L., S.A.-U., L.L., and D.J.K. designed research; C.L., D.V., and S.A.-U. performed research; C.L., D.V., S.A.-U., L.L., and D.J.K. analyzed data; and C.L., D.V., S.A.-U., L.L., and D.J.K. wrote the paper.

The authors declare no competing interest.

This article is a PNAS Direct Submission.

[1]To whom correspondence may be addressed. Email: l.laan@tudelft.nl or kraft@physics.leidenuniv.nl.

This article contains supporting information online at https://www.pnas.org/lookup/suppl/doi:10.1073/pnas.2106036118/-/DCSupplemental.

Published August 31, 2021.

comprehensive framework for multivalent interactions in biologically relevant settings. In particular, we expect that direct visualization of the spatial distribution of surface-mobile ligands and receptors will provide insights into their dynamics and impact on superselective surface binding.

Here, we introduce a colloid-based model system that allows direct investigation of the individual ligand–receptor interactions in a multivalent bond and their collective binding behavior to a target surface. We achieve this using fluorescently labeled double-stranded DNA with a single-stranded overhang that can hybridize with the complementary sequence, anchored in a lipid membrane on the colloids as well as the target surface. We observe that the colloid-target surface binding is mediated by the accumulation of receptors and ligands in the contact area. Interestingly, on the multivalent interaction timescale, individual ligand–receptor bonds dissolve and reform repeatedly. This dynamic reversibility confirms that the individual interactions are weak, in agreement with our observation of superselective binding at a critical ligand and receptor density. Our results motivate the development of theoretical models that link individual ligand–receptor dynamics to colloid–membrane binding and to reconcile effects taking place on the molecular scale with those on the micrometer scale.

Multivalent Bond Design and Visualization

Our multivalent experimental model system consists of colloidal probe particles functionalized with ligands and a surface featuring complementary receptors (Fig. 1*A*). Both the colloidal probe particles (2.12 ± 0.06-μm silica spheres) and the glass surface are coated with a supported lipid bilayer (SLB) and functionalized with DNA linkers as the ligand–receptor system. Each DNA linker consists of a 77 basepair (bp) double-stranded stem, which is modified with cholesterol on one $5'$ end to facilitate anchoring in the lipid membrane. Attached to the double-stranded stem, the linkers feature a single-stranded overhang (sticky end) whose length and complementary base pair sequence provide precise control over the tuneability of the hybridization free energy. *SI Appendix, Methods* has details. The integration into a lipid membrane both on the colloidal probe and on the surface provides full mobility of ligands and receptors if the lipid membrane is in the fluid state (26).

To visualize and quantify the multivalent colloid-surface binding, we employ a combination of total internal reflection fluorescence (TIRF) microscopy with Foerster resonance energy transfer (FRET) (27). We place fluorophores, which are also FRET pairs, on the $3'$ end of the complementary DNA linkers (Fig. 1*A*) and use dual-color imaging with alternating laser excitation to investigate the DNA–DNA interactions in the colloid-surface contact area. The separate imaging of the channels provides information on the ligand and receptor distribution on the surface (Fig. 1*B*). Upon binding, the intensity of the ligand and receptor signal increases on both the colloid and surface, and importantly, an FRET signal appears (Fig. 1*B*). We verify that the FRET signal corresponds to the presence of a colloidal probe by overlaying it with a bright-field image (Fig. 1*B*). The detection of the fluorescent and FRET signal is crucial to distinguish bound from unbound particles. The extended fluorescent patch in the contact area implies a local increase in the concentration of ligands and receptors and originates from the recruitment of the surface-mobile DNA linkers to the contact area. The simultaneous appearance of the FRET signal indicates that there are multiple ligand–receptor interactions between the colloidal probe and the surface and shows that our system is multivalent. With this experimental setup, which combines tunable ligand and receptor densities, mobile binding sites, and adjustable interaction strength (Fig. 1*C*), we can control and investigate the thermodynamic parameters relevant for superselective binding of multivalent colloids to a target surface and gain insights on the ligand–receptor dynamics on the molecular level.

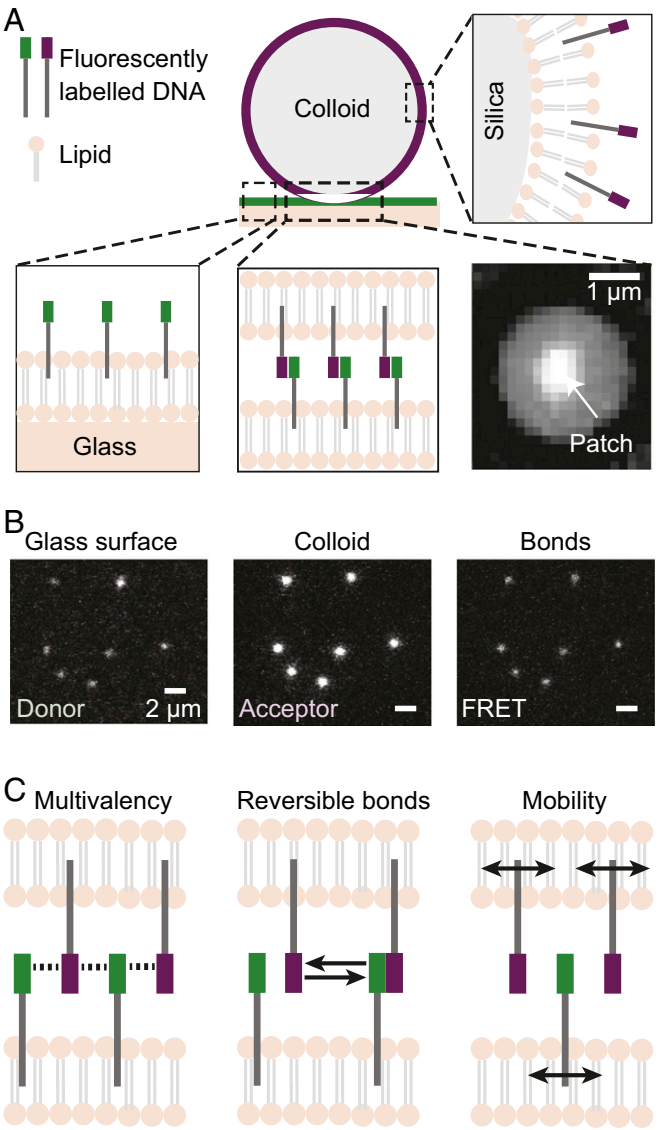

Fig. 1. Experimental model system. (*A*) The two-dimensional experimental system consists of 2.12-μm silica colloids functionalized with double-stranded DNA stems with a single-stranded linker overhang as the ligand and receptor system. The DNA strands are anchored in a lipid membrane on both the colloid and flat glass surface, which ensures their full mobility on the surface. (*B*) We separately detect the fluorescent signal of the receptor (*Left*) and ligand (*Center*) DNA strands, as well as the FRET signal emitted by bound ligand–receptor pairs (*Right*). The presence of a bright patch in the FRET channel indicates that a multivalent bond has been formed between the colloid and the surface. (*C*) Our model system features surface mobility of both ligands and receptors and allows us to tune the number of ligands and receptors (valency) as well as the interaction strength to systematically study superselective colloid-surface binding on the ligand–receptor level.

Nonlinear Binding Probability as a Function of Ligand Density

The hallmark of superselective binding is a sharp, nonlinear change of the binding probability in a specific ligand or receptor density range. We start by investigating the colloid-surface binding probability with increasing ligand density, σ_L, while keeping the receptor density, σ_R, on the surface fixed. Furthermore, we keep the overall DNA density constant on the colloidal probe and the target surface by the addition of 77-bp double-stranded

DNA that does not possess a sticky end. This ensures a constant concentration of cholesterol in the lipid membrane and hence, constant membrane properties (28–30). At low σ_L, the fluorescent signal is homogeneously distributed over the colloid and the target surface, and we do not observe fluorescent patches or an FRET signal (Fig. 2*A*). This indicates that binding does not occur despite the availability of DNA linkers on both colloid and surface. An increase of the ligand density on the colloid leads to the formation of patches on some probe particles, which implies that a fraction of the colloids in the sample is bound to the surface. Upon a further increase in σ_L, we observe that all colloids that are in close proximity to the membrane display a patch. The intensity of the patch differs between colloids, which is possibly due to the variability of ligand density between the functionalized colloids (31, 32). Additionally, the size of the patch at the highest ligand density shown in Fig. 2*A* spans an area of $\approx 0.37\ \mu m^2$. If we expect the patch to be circular, we can estimate the patch area $A_p = 2\pi R_c L$, where R_c is the colloid radius and L is the total bond length, yielding $A_p \approx 0.37\ \mu m^2$, which agrees very well with the measured patch area. The binding probability increases with the ligand concentration; however, superselectivity requires this transition to be nonlinear.

Therefore, we determine the number of bound particles, N_B, relative to the total number of colloids, N_C, to measure the binding probability, $\Theta = \frac{N_B}{N_C}$. A value of Θ equal to 0 implies that no colloids are bound, whereas the upper limit of $\Theta = 1$ is set by all colloids being bound to the surface. Other than varying the ligand density on the colloidal probe, we tested the binding behavior for four different interaction strengths (i.e., for four different sticky ends). We find that the binding probability smoothly transitions from an unbound to a bound state and saturates at high ligand densities, shown in Fig. 2*B*. Unexpectedly, saturation occurs slightly below $\Theta = 1$, even for very high ligand densities. A possible explanation for this observation is that at a certain ligand density, the binding free energy increases slower compared with the steric repulsion of the receptors, leading to a maximum Θ smaller than one (33), and even an eventual drop instead of saturation.

The range of ligand densities where the transition occurs depends on the interaction strength; the higher the interactions strength or the longer the sticky end, the fewer ligands are required for binding the colloid to the surface. In addition, the slope of this transition becomes steeper for weaker ligand–receptor interactions, indicating a higher sensitivity of the binding probability to the ligand density.

We examined the selectivity of the colloid binding for each binding probability curve by evaluating the relative change in binding probability with respect to a change in the ligand density σ_L, also known as the selectivity parameter $\alpha = \frac{\mathrm{d}\ln(\Theta)}{\mathrm{d}\ln(\sigma_L)}$ (16). The system is superselective in a specific ligand density range if $\alpha \gg 1$. In order to evaluate α for the different sticky ends, we first need a mathematical description of $\Theta(\sigma_L)$. A physically justified analytical form based on statistical mechanics considerations can be built by adapting a model first described by Martinez-Veracoechea and Frenkel (16). In this model, the binding probability Θ is written as

$$\Theta = \frac{zq(N_L, N_R, G_{\mathrm{bond}})}{1 + zq(N_L, N_R, G_{\mathrm{bond}})}, \qquad [1]$$

where $z = \rho_B v_{\mathrm{bind}}$ is the multivalent particle activity in a (diluted) solution, ρ_B is its bulk density, and v_{bind} is the

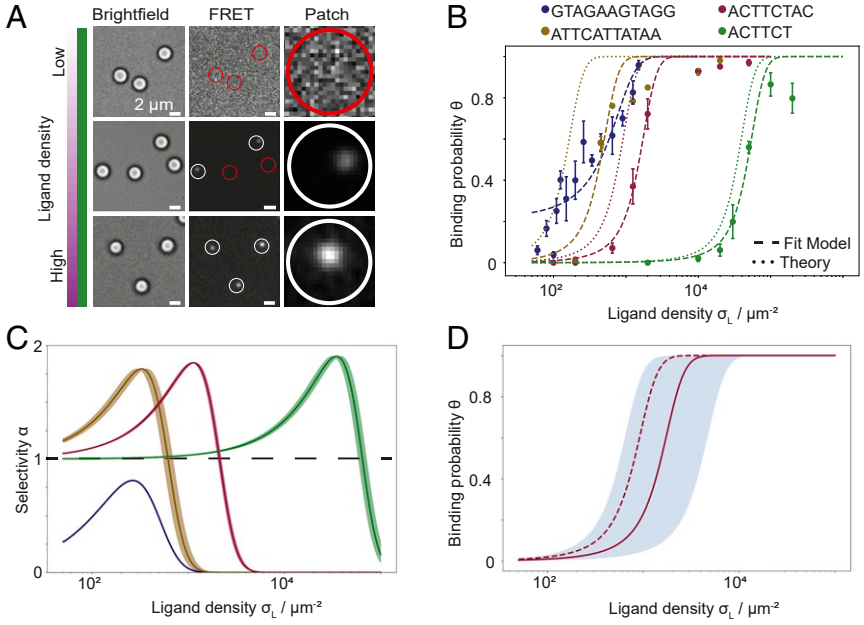

Fig. 2. Superselective surface binding. (*A*) Combining the information of the colloid position obtained from bright-field imaging with the FRET signal from bonded ligand–receptors allows us to discriminate whether a colloid-surface bond, a patch, has been formed. With increasing ligand density on the colloids, larger and more bond patches are formed, implying an increase in the binding probability Θ. The dynamic range between FRET images was individually adjusted to achieve an optimal visualization of the patch. (*B*) Measured colloid-surface binding probability Θ as a function of ligand density σ_L for different ligand–receptor interaction strengths tuned by varying the length of the single-stranded end. Dashed lines are least square fits to the model from Martinez-Veracoechea and Frenkel (16); dotted lines represent the adsorption profile obtained using a theoretically computed ΔG_{tot}. The data with the longest sticky end GTAGAAGTAGC are fitted with a logistics function. Increasing binding strength shifts the curves to the lower ligand densities. The good agreement between fitting and theoretical evaluation is even more remarkable considering that errors in binding energies are greatly amplified. The error bars represent the SE of at least three individual experiments. (*C*) The change in binding probability with ligand density can be measured by the selectivity parameter $\alpha = \frac{\mathrm{d}\ln(\Theta)}{\mathrm{d}\ln(\sigma_L)}$ and was derived from the fits in *B*. The shaded regions show the upper and lower boundaries of α resulting from the least square fit error for the binding free energy $\Delta G^{\mathrm{fit}}_{\mathrm{bond}}$. (*D*) Sensitivity of the fitting model. The solid and dashed lines are the same as in *B*; the shaded region shows the error bar for an uncertainty of $\pm 1 k_B T$.

binding volume: that is, the volume the particle center of mass can move in while being able to form bonds to the surface. In this expression, a central role is that of $q(N_L, N_R, G_{\mathrm{bond}})$, the ratio between the partition function in the bound and unbound states, which depends on the total number of ligands on the colloid and receptors on the surface, N_L and N_R, respectively, as well as their binding (free) energy, G_{bond}. In our case, a simple mean-field approximation (details are in *SI Appendix*) leads to the formula

$$q(N_L, N_R, G_{\mathrm{bond}}) = [1 + N_R \exp(-\beta G_{\mathrm{bond}})]^{N_L} - 1, \qquad [2]$$

with $\beta = k_B T$ where k_B is the Boltzmann constant and T is the temperature. Introducing a threshold detection value for the number of ligand–receptor bonds to the theory does not change the results in any statistically significant way (i.e., its effect is below the noise introduced by experiments). Therefore, we here used the simpler version of the model (*SI Appendix*). In this model, a bound state is any state where at least one bond is present, as we measure in our experiments. The binding strength of the multivalent system is incorporated in q, which takes into account all possible binding configurations of the ligands and receptors, as well as information regarding the average strength of a single ligand–receptor bond, measured by $\exp(-\beta G_{\mathrm{bond}})$. Notably, in our system the bond strength is affected by experimental parameters such as the size of the rigid, double-stranded stem of the DNA and the sequence of the single-stranded part (sticky end) as well as DNA mobility on the colloid (34). In particular, the latter introduces a dependence of the effective bond strength on the colloids area, as well as on that of the surface on which receptors are grafted (35). The exact value of G_{bond} can be calculated via detailed molecular simulations or experiments. Here, we leave it as a fitting parameter, and then compare the fitted value with an approximate theoretical expression derived by Mognetti et al. (36) for mobile ligands and receptors and adapted here for our system. Within this framework, we obtain

$$G_{\mathrm{bond}} = G_0 + G_{\mathrm{conf}} = G_0 + k_B T \log(2 R_c A_{\mathrm{tot}} \rho^{\circ}), \qquad [3]$$

where G_0 is the binding energy of the sticky end of the DNA in solution [which can be accurately estimated via SantaLucia's nearest-neighbor rules (37)] and G_{conf} is the so-called configurational contribution to the bond energy (34). In our system, this last term turns out to be only dependent on the colloid radius R_c, the total binding surface A_{tot}, and the reference molar concentration $\rho^{\circ} = 1\mathrm{M}$ (details are in *SI Appendix*). Importantly, using Eq. **3** the binding probability Θ is fully determined, leaving no fitting parameter.

The results of fitting the experimental data on the binding probability as a function of the ligand density are reported in Fig. 2, along with the experimental data. We do this by using the expression where G_{bond} is left as a fitting parameter, which we will refer to as the free model, as well as the full theory. The fabrication process of ligand-coated colloids leads to a variability in the number of ligands per particle. Although including the effect of variability in the analytical model could be done in principle (e.g., ref. 16), to avoid introducing artifacts, the measured distribution should be used instead of assuming a specific analytical form, which is not known for our samples. At the same time, the inclusion of a probability distribution describing the variability would not change the trends that we observe. Because of these reasons, we neglect ligand fluctuations in our model. In the steep regime where α is determined, the fit model nicely captures the experimental data for all sticky end sequences but the strongest one. For the strongest binding sequence ($\Delta G^0 = -17 k_B T$), however, the predicted trend is steeper than what is observed experimentally, and for this reason, the theoretical model cannot be relied on to calculate the value of the superselectivity parameter α. Thus, we use an empirical logistic function with two parameters for this case (Fig. 2*B*). The decrease in predictive power of the theoretical expression for increasing bond strengths is expected because the theoretical model is based on equilibrium considerations, where we assumed that binding and unbinding are fast enough for a colloid to fully sample all its possible binding configurations. However, this assumption becomes less and less justified as the bond lifetime increases, an increase expected to be exponential in terms of G_0.

For the range of parameter in which the equilibrium model well describes the experimental data, we can compare the fit model with the full theory (Table 1). The agreement is remarkable, as the full theory provides a value for the only fitting parameter in the fit model, the bond energy G_{bond}, which only deviates from the one obtained through least squares fitting by $\approx 1 k_B T$. Notably, even such a small discrepancy can result in a relatively large shift of the predicted adsorption probability because of the extreme sensitivity of the latter to G_{bond}, as illustrated in Fig. 2*D*, where the shaded region corresponds to the predicted curve obtained given an uncertainty of $1 k_B T$ on the bond energy.

Having fitted the data with an analytical form, we can easily compute the selectivity α (Fig. 2*C*). Each sticky end shows a maximum selectivity for a specific ligand density. For the three sticky ends ATTCATTATAA ($\Delta G^0 = -13 k_B T$), ACTTCTAC ($\Delta G^0 = -11 k_B T$), and ACTTCT ($\Delta G^0 = -7 k_B T$), we observe $\alpha \gg 1$, indicating that the colloid-surface binding is superselective. We note that a distribution in the number of ligands per particle across the sample decreases the slope in the binding probability curve. Hence, finding superselective behavior in our sample of colloids with such a distribution implies evidence that the superselectivity parameter α for a sample with a narrower distribution is in fact even higher. The longest and hence, strongest binding sticky end GTAGAAGTAGG ($\Delta G^0 = -17 k_B T$), however, does not exceed $\alpha = 1$ and is thus not superselective. The results of the binding probability for different ligand densities and interaction strengths show the relevance of employing weak interactions to achieve superselective binding in multivalent systems, as previously pointed out by Martinez-Veracoechea and Frenkel (16).

Nonlinear Binding Probability as a Function of Receptor Density

Increasing the number of receptors on the flat surface changes the entropic effects upon binding and can increase the sensitivity of colloid-surface binding, similar to a change in ligand density. Here, we tune the selectivity of colloid-surface binding by changing the receptor density on the surface while keeping the ligand density constant and at the same time, investigating

Table 1. Comparison between the binding free energy obtained from the multivalent model and experimental data

Free energy (k_BT)	ΔG^0	ΔG^{fit}(lig)	ΔG^{fit}(rec)	ΔG^{theo}	$\lvert\Delta G^{\mathrm{fit}} - \Delta G^{\mathrm{theo}}\rvert$
ACTTCT	−7	32	N/A	31	1 − N/A
ACTTCTAC	−11	28	N/A	28	0 − N/A
ATTCATTATAA	−13	27	25	26	1 − 1
GTAGAAGTAGG	−17	27	24	21	6 − 3

The binding free energy ΔG_{bond} is obtained for the four sticky ends by computing the theoretical value (ΔG^{theo}) (*Materials and Methods*) and by fitting Eq. **1** to the binding curves for a variation in the ligands (Fig. 2), ΔG^{fit}(lig), and receptors (3), ΔG^{fit}(rec). The absolute differences between the experimental and theoretical values $\Delta G^{\mathrm{fit}} - \Delta G^{\mathrm{theo}}$ are shown in the last column; the first value in each row is obtained using the experimental value of the free energy obtained varying the concentration of ligands ΔG^{fit}(lig), while the second is computed using ΔG^{fit}(rec). These differences are small with respect to thermal energy k_BT, verifying that our model is appropriate for our experimental setup. N/A, not available.

if the colloids indeed bind superselectively to a surface. We quantify the binding probability for two 11-bp sticky ends ATTCATTATAA ($\Delta G^0 = -13 k_B T$) and GTAGAAGTAGG ($\Delta G^0 = -17 k_B T$) at a fixed ligand density of 1,250 μm^{-2} (Fig. 3*A*). Similar to a change in ligand density, we observe an increase of the binding probability until it saturates around $\Theta = 1$.

We use the same physical model to evaluate the binding probability as well as the superselectivity parameter by fitting the experimental data, finding again good agreement between theory and experiments (Fig. 3*A*). We note that in this case the selectivity parameter for both 11-bp sticky ends is larger than one in a specific receptor density range, and thus, both systems are behaving superselectively. Interestingly, in this case the sticky end GTAGAAGTAGG binds superselectively, whereas this was not observed in the system with fixed receptor density and varying ligand density. We hypothesize that the asymmetry of the experimental system in combination with the surface mobility of the DNA linkers can explain these observations; the maximum number of ligands available for binding is constrained by the finite surface area of the colloid, whereas the number of receptors that can be recruited to the binding area is only limited by the geometric constraints in the binding area itself. This should affect the combinatorial entropy contribution and hence, the superselective binding behavior in two ways: 1) directly through fewer available binding partners at a given ligand density compared with the same receptor density, but also, 2) indirectly when the timescale for sampling all possible binding configurations increases for lower ligand densities because the relative number of ligands available for binding is lower, which would decrease the binding probability in Fig. 2*B*. Hence, we suspect that a high valency on the colloid leads to a faster bond formation and thus, equilibration of the system, which can explain this observation. These results indicate that the binding kinetics play an important role in multivalent bond formation.

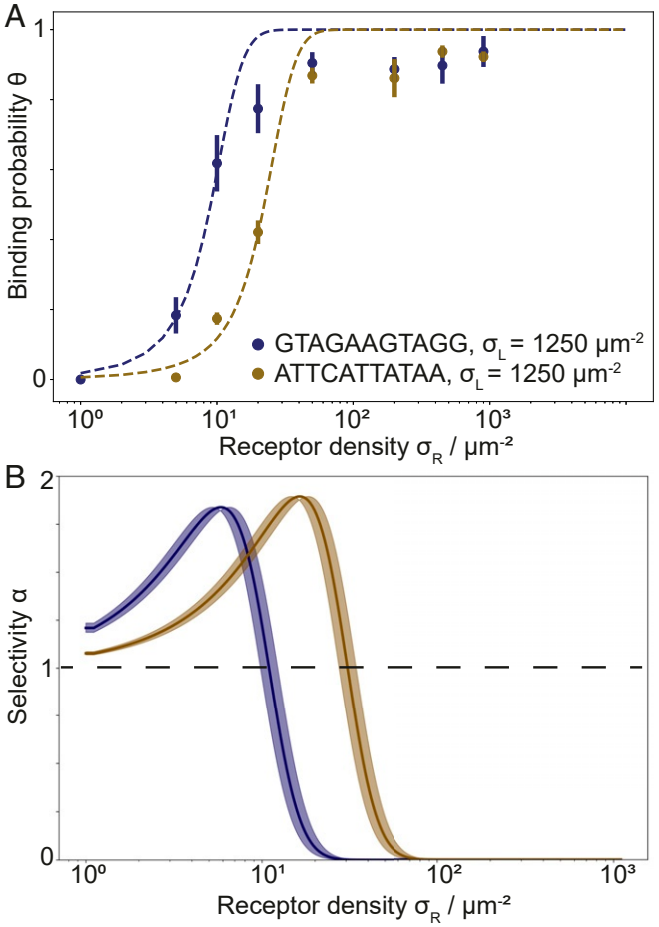

Fig. 3. Multivalent binding as a function of the receptor density. (*A*) Binding probability as a function of the receptor density for the 11-bp sticky ends GTAGAAGTAGG and ATTCATTATAA at fixed ligand density of 1,250 μm^{-2}. The error bars represent the SE of at least three individual experiments. (*B*) Selectivity parameter α resulting from a fit with the physical model shows a superselective regime with $\alpha > 1$ for both sticky ends. The shaded regions show the upper and lower boundaries of α, resulting from the least square fit error for the binding free energy $\Delta G^{\text{fit}}_{\text{bond}}$.

Binding Kinetics

For superselectivity to be observed on a given timescale, the dynamics of the individual bonds need to be fast enough for them to behave reversibly on that timescale. In other words, bonds should constantly form and break. In fact, if bonds were irreversible, the binding probability would be one regardless of the density of ligands and receptors.

Since our setup allows for the direct visualization of the spatial receptor distribution on the flat surface, we can visualize the exchange of the receptors inside the contact area with unbound receptors in close proximity of the patch using fluorescent recovery after photobleaching (FRAP) (Fig. 4*A*). We performed bleaching experiments of ligand–receptor patches in the contact area for three sticky ends ACTCTAC ($\Delta G^0 = -11 k_B T$), ATTCATTATAA ($\Delta G^0 = -13 k_B T$), and GTAGAAGTAGG ($\Delta G^0 = -17 k_B T$) and recorded the signal recovery up to 300 s (Fig. 4*B*). After bleaching the receptors in the patch, we observe a recovery of the signal for all sticky ends, albeit at different rates. Furthermore, the recovery rate depends on the sticky end; the stronger the hybridization free energy, the longer the recovery of the receptor signal takes. This shows that the hybridization energy of the individual receptors and ligands influences the timescale on which the formation and dissolving of bonds occur.

Mathematical modeling allows us to unravel some details of the kinetics in our system and gauge the relative importance of different processes in the observed behavior. At a coarse-grained level, the intensity recovery over time for our system should be well described within the framework of Langmuir kinetics (38), whose assumptions we use here to derive a simple two-component model (corresponding to the description of bleached vs. unbleached DNA) to gain a better, quantitative understanding of the dynamics of receptor–ligand bonds in the patch. Within this model, the normalized intensity I as a function of time after bleaching is given by (*SI Appendix* has details)

$$I = \frac{k_{\text{in}}\sigma_0}{k_{\text{out}} + k_{\text{in}}\sigma_0}\left(1 - e^{-k_{\text{out}}t}\right) + I_0\, e^{-k_{\text{out}}t}, \qquad [4]$$

where k_{in} and k_{out} are two kinetic constants related to the inward and outward flux of receptors from the bulk to the patch and vice versa, respectively; σ_0 is the bulk density of receptors on the surface; and I_0 is the initial value of the intensity, which is not always exactly zero due to partial bleaching of the patch. The initial speed of recovery under our experimental conditions is approximately proportional to the product $k_{\text{in}}k_{\text{out}}\sigma_0$, which we use to quantify the speed at which systems employing different ligand–receptor pairs reach dynamical equilibrium (again, *SI Appendix* has details). The exact relation between microscopic details of the system and the values of k_{in} and k_{out} is difficult to quantify without the use of accurate molecular simulations. For example, the speed at which receptors can diffuse will be dependent on the viscosity of the lipid membrane and the interaction

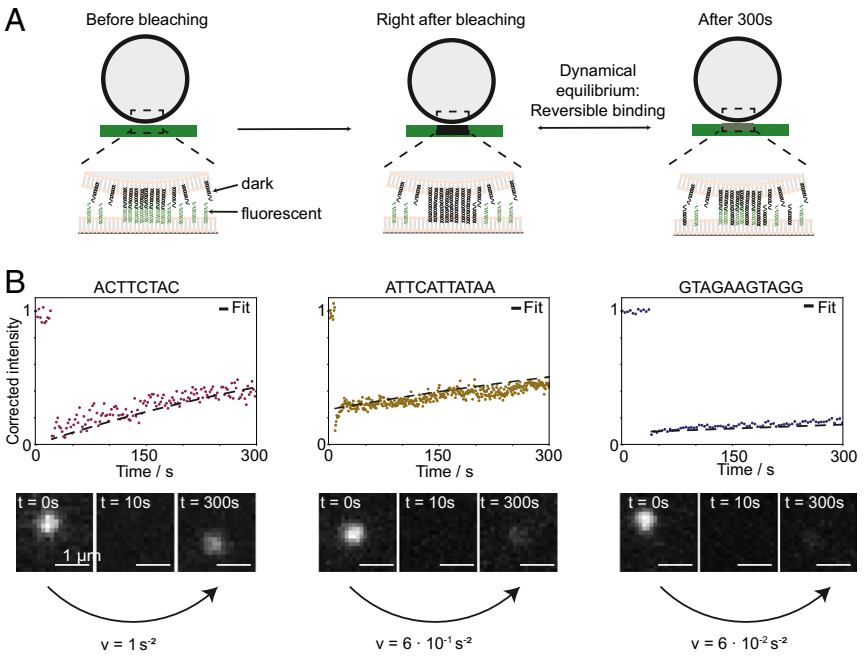

Fig. 4. Ligand–receptor binding kinetics in a multivalent bond. (*A*) Receptors and ligands with weak interactions repeatedly break and form bonds over time. We visualize their dynamic binding and unbinding by observing the FRAP of the receptors in the contact area of a colloidal particle and the target surface. For sufficiently weak ligand–receptor interactions, the bonded pairs frequently break, and bleached receptors can diffuse out of the patch with a flux $\propto k_{out}$. At the same time, unbleached receptors can diffuse into the patch with flux $\propto k_{in}$ and bind to ligands on the colloid. This exchange results in an increase of the receptor signal of the patch in time. (*B*) FRAP experiments for three sticky ends. *Upper* shows intensity recovery in time; *Lower* shows the recovery of the fluorescent intensity in the receptor channel in time. Colloidal probes coated with the sticky end ACTTCTAC have a ligand density of 100,000 μm^{-2}, and colloids coated with the 11-bp sticky end comprise 10,000 μm^{-2} ligands. The target surface was functionalized with a receptor density of 450 μm^{-2}. Fitting the FRAP curves with Eqs. **4**–**6**, we can quantify the initial speed of recovery, which is defined as the product $\nu = \sigma_0 k_{out} k_{in}$.

between cholesterol linkers and lipid chains. Here, instead, we therefore only provide an approximate expression showing how the kinetic constant is expected to depend on parameters such as the receptors diffusion coefficient in the lipid membrane D and the sticky end hybridization free energy G_0, which reads

$$k_{\text{in}} = \gamma_1 D \qquad [5]$$

$$k_{\text{out}}^{-1} = k_{\text{diff}}^{-1} + k_{\text{break}}^{-1} = \gamma_2 R_c L/D + \gamma_3 \exp(-\beta G_0), \qquad [6]$$

where γ_i, $i = 1, 2, 3$ are system-dependent constants within our model, which we will use to fit our experimental data, and L is the length of the receptor. We obtained these approximate formulas by assuming that k_{in} depends on the rate at which ligands from the outside of the binding patch diffuse into it, whereas k_{out} arises from a two-step process, where the bound ligand–receptor pairs in the patch first unbind and later, the receptor diffuses out of the binding patch, whose size will be of the order of $R_c L$ (*SI Appendix* has details). Given their origin from the solution of a diffusion problem and based on dimensional analysis, γ_1 and γ_2 should be nondimensional coefficients of order one and only dependent on geometrical factors (i.e., the specific boundary conditions under which the ligands evolve). Because the sticky ends are located at the top of a long double-stranded DNA stem, they will be mostly far from the lipid membrane, and we do not expect them to strongly influence the diffusion coefficient of different ligands and receptors.

For this reason, we fix $\gamma_1 = \gamma_2 = 1$ for all the systems investigated. In contrast, γ_3 has the dimensions of a time and can be thought of as the natural bond lifetime of a bond of $G_0 = 0$. Because γ_3 is expected to be a function of the exact microscopic details of the bond-breaking mechanism, we leave it as a system-specific fitting parameter. Thus, k_{in} will be constant by construction for all ligands and receptors, while we expect k_{out} to decrease as the bond between the sticky ends of the DNA becomes stronger, due to its dependence on G_0.

A fit of Eq. **4** to the intensity recoveries yields the unknown parameter k_{out} (Fig. 4*B*). As expected, the product $k_{\text{out}} k_{\text{in}}$, which quantifies the initial speed of recovery, shows a decrease with increasing bond strength. A more detailed analysis of the fitting results provides two crucial physical insights; the first is that the quality of the fitting is essentially insensitive to the value of k_{in}, whereas it strongly depends on k_{out} (*SI Appendix*, Fig. S1). This suggests that a correct description of the process by which receptors diffuse out of the binding patch is more important than diffusion toward it. To make this more quantitative, we calculate the nondimensional parameter $\delta = \frac{k_{\text{in}} \sigma_0}{k_{\text{out}}}$ as a measure of the relative magnitude of the ingoing vs. outgoing flux toward the patch (*SI Appendix*, Table S1). For all sequences used here, $\delta \gg 1$, showing that the outward diffusion is much slower than inward diffusion and implying that it is the bottleneck of the signal recovery process.

Second, we find that $k_{\text{diff}} \gg k_{\text{break}}$. Interpreted in light of the model expressed in Eqs. **5** and **6**, this suggests that the kinetics in our system are dominated by bond breaking rather than diffusion. In other words, bond breaking is the rate-limiting factor for the system to sample different binding configurations. This is an important finding since superselectivity has been shown to arise from statistical mechanical effects, in particular the steep increase in the combinatorial entropy of binding as the number of ligands and receptors increases. To observe an ergodic sampling of these configurations within the timescales accessible to experiments, and thus observe superselective behavior (which is an equilibrium property), requires the system dynamics to happen on much shorter timescales. Here, we have shown that,

at least for our system, these are dominated by the unbinding kinetics of the ligand–receptor pair. Similar findings have been reported in a recent study focusing on the mode of diffusion of ligand-coated colloid exhibiting interparticle linkages (39).

Conclusion

Multivalent binding in a fully mobile system is a highly dynamic process that can show superselective surface binding at the right ratio of enthalpic and entropic contributions. In this work, we have combined experiments with theory to investigate the binding probability of multivalent ligand and receptor interactions between two surfaces that provide full mobility to the ligands and receptors. Our experimental setup allowed us to directly visualize the spatial distribution of the individual binding sites. We have shown that multivalent binding between fluid surfaces is characterized by receptor and ligand clustering as suggested by Lanfranco et al. (20) and Dubacheva et al. (19). Following the design rules proposed by Martinez-Veracoechea and Frenkel (16), we demonstrated that we can achieve superselective binding by tuning the hybridization energy of the individual ligands and receptors and measured the effective free energy of binding. Finally, we visualized and quantified the reversibility of weak bonds through the highly dynamic exchange of bound receptors with unbound ones from outside the binding patch.

Future studies with this model system can provide exciting insights into the binding kinetics of multivalent interactions at the ligand–receptor level, for example, the formation of bonds and development of the spatial distribution in time. The observed timescale of bond formation and importance of the timescale for bond breakage might be crucial for competitive binding of various receptors on cell surfaces. Moreover, our experimental system can provide insights into membrane deformations caused by locally high receptor and ligand accumulations, which is important for the initiation of endocytosis. Surface targeting in biological systems is often governed by more than one type of receptors and ligands, and our model system can straightforwardly be extended to study the effect of competing interactions between more types of ligands and receptors on superselectivity (40–42). Finally, our experimental system might provide key insights for applications in nanomedicine as it can be used to improve specific target binding while reducing off-target binding, useful, for example, for drug delivery.

Materials and Methods

DNA Strands. All DNA strands (Integrated DNA Technologies, Inc.; Eurogentec; IBA) with a sticky end are functionalized with cholesterol at the 5′. The 3′ is modified with a fluorophore (*Cy3*/*Cy5*, *Cy3*/*Atto655*). The complementary backbone DNA strand had a length of 77 bp and cholesteryltriethylene glycol at the 3′ end. Single-stranded DNA with the sticky end and single-stranded backbone were annealed to 95°C and slowly cooled in 0.2°C/min steps in Tris acetate-EDTA (ethylenediaminetetraacetic acid)-NaCl (TAE; 100 mM NaCl, pH = 8; Formedium) buffer in a Thermocycler. The resulting DNA strands are double stranded with a double-cholesterol anchor and a single-stranded overhang. The hybridized DNA strands were stored in TAE-NaCl buffer at 4°C. The single-stranded overhang varies in sequence and length with a hybridization energy ranging between $\Delta G^0 = -7k_BT - (-17k_BT)$ (43). The sticky ends used as the ligand and receptor system are ACTTCT, ACTTCTAC, ATTCATTATAA, GTAGAAGTAGG, and their respective complementary sequences (*SI Appendix*, Table S2).

DNA-Coated Colloid SLBs. We coated commercial silica spheres (Microparticle GmbH) of 2.12 μm with an SLB. To do so, we mixed the silica particles (0.5wt%) with SUVs consisting of the desired lipid composition and incubated the mixture at room temperature for 30 min. To obtain the SUVs, we first added the desired volume of 18 : 1 (Δ 9-Cis) 1,2-dioleoyl-*sn*-*glycero*-3-phosphocholine lipids (Avanti Polar Lipids; stored in chloroform) into a glass vial and let it dry overnight in a vacuum desiccator. Next, we resuspended the dried lipids in TAE-NaCl buffer and extruded the solution with an Avanti mini extruder through a membrane with pore size of 30 nm, yielding a transparent solution. By mixing the SUVs with the colloids, the SUVs spread on the colloid surface to form an SLB. Excess SUVs were removed by centrifugation of the mixture at 2,000 *g* for 30 s and subsequent replacement of the supernatant with fresh TAE-NaCl buffer. The desired concentration of hybridized DNA was added to the colloid-supported lipid bilayers (CSLBs) and incubated for 1 h at room temperature (26, 44). Using the stock concentration and surface area of the colloids in solution, we estimated the final DNA surface density σ_{DNA} on the CSLB, which typically ranged between 60 and 100,000 μm^{-2}. After the incubation time, we washed the mixture trice by centrifugation at 2,000 *g* for 30 s and replacement of the supernatant with fresh buffer. The last replacement of the supernatant was done with imaging buffer (0.8% dextrose, 1 mg/mL glucose oxidase, 170 mg/mL catalase, and 1 mM Trolox [(±) − 6 − hydroxy − 2, 5, 7, 8 − tetramethylchromane − 2 − carboxylic acid; 238813; Merck]) (45) to reduce the bleaching of the fluorophores during imaging.

DNA Functionalized the SLB on a Flat Glass Surface. The microscopy slides and coverslips were sonicated for 30 min each in 2% Hellmanex, acetone (> 99.9%), and potassium hydroxide solution (KOH 1 M; Merck). Between each change of chemical, the glassware was rinsed with milliQ water and blown dry with nitrogen before use. The experiments were performed in a flow channel consisting of parafilm slices between a glass microscope slide (VWR) and a glass coverslip (VWR). Placing the construct on a heating stage at 125°C melted the parafilm and bound the objective slide and coverslip together, yielding four 2- × 24-mm flow channels. Before we injected SUVs into the flow channels, we cleaned the channels with TAE-NaCl buffer. After 30 min, we washed out the excess SUVs with TAE-NaCl buffer and added DNA with the complementary DNA sequence at the desired concentration with respect to the DNA CSLB. Here, the resulting DNA surface densities σ_{DNA} used varied between 5 and 1,500 μm^{-2}. After 1 h of incubation, we flushed the channels three times with TAE-NaCl buffer before injecting the DNA CSLBs to the flow channels.

Total Internal Reflection Microscopy. The colloidal silica particles quickly sedimented to the flat SLB due to their density being higher than that of water. To image the colloid–membrane interactions, we used TIRF microscopy on an inverted fluorescence microscope (Nikon Ti2-E) upgraded with an azimuthal TIRF/FRAP illumination module (Gataca Systems iLAS 2) equipped with a 100× oil immersion objective (Nikon Apo TIRF; 1.49 numerical aperture). To investigate the DNA–DNA interactions in the colloid-surface contact area, we used dual-color imaging with alternating laser excitation with wavelengths 561 and 640 nm (Cairn Research Optosplit II ByPass; EM-CCD Andor iXON Ultra 897). This technique allowed for alternating excitation of the donor and receptor, yielding an FRET when the two complementary DNA linker strands hybridized. Subsequently, we acquired a bright-field image to localize the colloids on the surface (CCD Retiga R1). This setup was also used to perform FRAP experiments to investigate the mobility of DNA in the membrane and patch. Per sample, we imaged 100 colloids in at least three independent experiments. The error bar on the binding probability represents the SEM. The error bar on the selectivity α results from the least square fitting error.

Image Analysis. After the acquisition of the data, we deinterleaved and cropped the resulting images with respect to the three fluorescent channels corresponding to the donor, acceptor, and FRET. For each measurement, we first acquired an image with fluorescent beads, which is used for the spatial calibration of the channels and the bright-field image. An ImageJ plugin (46) was used to overlay the fluorescent channels with the bright-field image to locate the DNA–DNA interactions with respect to the colloids. We defined a colloid bound to the flat surface via DNA–DNA interactions if we could visually differentiate the signal in the colloid-surface contact area of the donor, acceptor, and FRET channel from the local background signal.

For the FRAP experiments, we extracted the intensity profile of the bleached area via ImageJ, and we first subtracted the background noise of the microscope and then normalized the raw intensity with respect to the initial unbleached intensity. Per condition, we imaged at least three patches and in three independent experiments.

Data Availability. Datasets and software have been deposited in 4TU.ResearchData (https://data.4tu.nl/; dataset [DOI: 10.4121/14350709] and software [DOI: 10.4121/14339588]).

ACKNOWLEDGMENTS. We thank Ramon van der Valk and Anne Schwabe for technical help and Jérémie Capoulade for help with microscopy. C.L.,

L.L., and D.J.K. acknowledge support from the Netherlands Organization for Scientific Research (NWO/OCW), as part of the Gravitation Program: Frontiers of Nanoscience. D.V. and S.A.-U. acknowledge the United Kingdom Materials and Molecular Modelling Hub, which is partially funded by Engineering and Physical Sciences Research Council Grant EP/P020194/1, for computational resources.

1. M. Mammen, S. K. Choi, G. M. Whitesides, Polyvalent interactions in biological systems: Implications for design and use of multivalent ligands and inhibitors. *Angew. Chem. Int. Ed. Engl.* **37**, 2754–2794 (1998).
2. J. Huskens, Multivalent interactions at interfaces. *Curr. Opin. Chem. Biol*. **10**, 537–543 (2006).
3. T. Satav, J. Huskens, P. Jonkheijm, Effects of variations in ligand density on cell signaling. *Small* **11**, 5184–5199 (2015).
4. N. J. Boudreau, P. L. Jones, Extracellular matrix and integrin signalling: The shape of things to come. *Biochem. J.* **339**, 481–488 (1999).
5. C. Fasting *et al*., Multivalency as a chemical organization and action principle. *Angew Chem. Int. Ed. Engl.* **51**, 10472–10498 (2012).
6. X. Tian, S. Angioletti-Uberti, G. Battaglia, On the design of precision nanomedicines. *Sci. Adv.* **6**, eaat0919 (2020).
7. M. Liu *et al*., Combinatorial entropy behaviour leads to range selective binding in ligand-receptor interactions. *Nat. Commun.* **11**, 4836 (2020).
8. S. Hauert, S. N. Bhatia, Mechanisms of cooperation in cancer nanomedicine: Towards systems nanotechnology. *Trends Biotechnol.* **32**, 448–455 (2014).
9. J. Wang, J. Min, S. A. Eghtesadi, R. S. Kane, A. Chilkoti, Quantitative study of the interaction of multivalent ligand-modified nanoparticles with breast cancer cells with tunable receptor density. *ACS Nano* **14**, 372–383 (2020).
10. J. Zhang, Z. Wang, Y. Gao, Z.-S. Wu, Simple self-assembled targeting DNA nano sea urchin as a multivalent drug carrier. *ACS Appl. Bio Mater* **3**, 4514–4521 (2020).
11. Y. Zhang *et al*., Multivalent nanoparticles for personalized theranostics based on tumor receptor distribution behavior. *Nanoscale* **11**, 5005–5013 (2019).
12. S. Li, S. Huang, S. B. Peng, Overexpression of G protein-coupled receptors in cancer cells: Involvement in tumor progression. *Int. J. Oncol.* **27**, 1329–1339 (2005).
13. M. J. Akhtar, M. Ahamed, H. A. Alhadlaq, S. A. Alrokayan, S. Kumar, Targeted anticancer therapy: Overexpressed receptors and nanotechnology. *Clin. Chim. Acta* **436**, 78–92 (2014).
14. P.-A. Koenig *et al*., Structure-guided multivalent nanobodies block SARS-CoV-2 infection and suppress mutational escape. *Science* **371**, eabe6230 (2021).
15. G. J. Doherty, H. T. McMahon, Mechanisms of endocytosis. *Ann. Rev. Biochem.* **78**, 857–902 (2009).
16. F. J. Martinez-Veracoechea, D. Frenkel, Designing super selectivity in multivalent nano-particle binding. *Proc. Natl. Acad. Sci. U.S.A.* **108**, 10963–10968 (2011).
17. G. A. Duncan, M. A. Bevan, Computational design of nanoparticle drug delivery systems for selective targeting. *Nanoscale* **7**, 15332–15340 (2015).
18. S. Wang, E. E. Dormidontova, Selectivity of ligand-receptor interactions between nanoparticle and cell surfaces. *Phys. Rev. Lett.* **109**, 238102 (2012).
19. G. V. Dubacheva, T. Curk, D. Frenkel, R. P. Richter, Multivalent recognition at fluid surfaces: The interplay of receptor clustering and superselectivity. *J. Am. Chem. Soc.* **141**, 2577–2588 (2019).
20. R. Lanfranco *et al*., Kinetics of nanoparticle-membrane adhesion mediated by multivalent interactions. *Langmuir* **35**, 2002–2012 (2019).
21. D. Di Iorio, Y. Lu, J. Meulman, J. Huskens, Recruitment of receptors at supported lipid bilayers promoted by the multivalent binding of ligand-modified unilamellar vesicles. *Chem. Sci. (Camb.)* **11**, 3307–3315 (2020).
22. G. V. Dubacheva *et al*., Superselective targeting using multivalent polymers. *J. Am. Chem. Soc.* **136**, 1722–1725 (2014).
23. G. V. Dubacheva, T. Curk, R. Auzély-Velty, D. Frenkel, R. P. Richter, Designing multivalent probes for tunable superselective targeting. *Proc. Natl. Acad. Sci. U.S.A.* **112**, 5579–5584 (2015).
24. M. R. W. Scheepers, L. J. van IJzendoorn, M. W. J. Prins, Multivalent weak interactions enhance selectivity of interparticle binding. *Proc. Natl. Acad. Sci. U.S.A.* **117**, 22690–22697 (2020).
25. N. J. Overeem *et al*., Hierarchical multivalent effects control influenza host specificity. *ACS Cent. Sci.* **6**, 2311–2318 (2020).
26. M. Rinaldin, R. W. Verweij, I. Chakraborty, D. J. Kraft, Colloid supported lipid bilayers for self-assembly. *Soft Matter* **15**, 1345–1360 (2019).
27. S. F. Shimobayashi *et al*., Direct measurement of DNA-mediated adhesion between lipid bilayers. *Phys. Chem. Chem. Phys.* **17**, 15615–15628 (2015).
28. R. C. Aloia, *Membrane Fluidity in Biology: Cellular Aspects* (Academic Press, 1985).
29. Y. Zhang, Q. Li, M. Dong, X. Han, Effect of cholesterol on the fluidity of supported lipid bilayers. *Colloids Surf. B Biointerfaces* **196**, 111353 (2020).
30. S. Chakraborty *et al*., How cholesterol stiffens unsaturated lipid membranes. *Proc. Natl. Acad. Sci. U.S.A.* **117**, 21896–21905 (2020).
31. P. Delcanale, B. Miret-Ontiveros, M. Arista-Romero, S. Pujals, L. Albertazzi, Nanoscale mapping functional sites on nanoparticles by points accumulation for imaging in nanoscale topography (PAINT). *ACS Nano* **12**, 7629–7637 (2018).
32. I. Chakraborty, V. Meester, C. v. d. Wel, D. J. Kraft, Colloidal joints with designed motion range and tunable joint flexibility. *Nanoscale* **9**, 7814–7821 (2017).
33. M. Liu *et al*., Combinatorial entropy behaviour leads to range selective binding in ligand-receptor interactions. *Nat. Commun.* **11**, 1–10 (2020).
34. P. Varilly, S. Angioletti-Uberti, B. M. Mognetti, D. Frenkel, A general theory of DNA-mediated and other valence-limited colloidal interactions. *J. Chem. Phys.* **137**, 094108 (2012).
35. S. Angioletti-Uberti, P. Varilly, B. M. Mognetti, D. Frenkel, Mobile linkers on DNA-coated colloids: Valency without patches. *Phys. Rev. Lett.* **113**, 128303 (2014).
36. B. M. Mognetti, P. Cicuta, L. Di Michele, Programmable interactions with biomimetic DNA linkers at fluid membranes and interfaces. *Rep. Prog. Phys.* **82**, 116601 (2019).
37. J. SantaLucia Jr., A unified view of polymer, dumbbell, and oligonucleotide DNA nearest-neighbor thermodynamics. *Proc. Natl. Acad. Sci. U.S.A.* **95**, 1460–1465 (1998).
38. S. Azizian, Kinetic models of sorption: A theoretical analysis. *J. Colloid Interface Sci.* **276**, 47–52 (2004).
39. P. K. Jana, B. M. Mognetti, Translational and rotational dynamics of colloidal particles interacting through reacting linkers. *Phys. Rev. E* **100**, 060601 (2019).
40. T. Curk, J. Dobnikar, D. Frenkel, Optimal multivalent targeting of membranes with many distinct receptors. *Proc. Natl. Acad. Sci. U.S.A.* **114**, 7210–7215 (2017).
41. D. Bray, M. D. Levin, C. J. Morton-Firth, Receptor clustering as a cellular mechanism to control sensitivity. *Nature* **393**, 85–88 (1998).
42. J. F. Stefanick, D. T. Omstead, T. Kiziltepe, B. Bilgicer, Dual-receptor targeted strategy in nanoparticle design achieves tumor cell selectivity through cooperativity. *Nanoscale* **11**, 4414–4427 (2019).
43. N. R. Markham, M. Zuker, DINAMelt web server for nucleic acid melting prediction. *Nucleic Acids Res.* **33**, W577–W581 (2005).
44. S. A. J. van der Meulen, M. E. Leunissen, Solid colloids with surface-mobile DNA linkers. *J. Am. Chem. Soc.* **135**, 15129–15134 (2013).
45. J. van Ginkel *et al*., Single-molecule peptide fingerprinting. *Proc. Natl. Acad. Sci. U.S.A.* **115**, 3338–3343 (2018).
46. S. Preibisch, S. Saalfeld, J. Schindelin, P. Tomancak, Software for bead-based registration of selective plane illumination microscopy data. *Nat. Methods* **7**, 418–419 (2010).